Papers

Volume 8: 2008-2014

Thoft-Christensen, Palle

Publication date:
2014

Document Version
Publisher's PDF, also known as Version of record

CHAPTER 142

NUMERICAL ESTIMATION OF FATIGUE LIFE OF WIND TURBINES DUE TO SHADOW EFFECT[1]

P. Thoft-Christensen, R.R. Pedersen & S.R.K. Nielsen
Aalborg University, Aalborg, Denmark

ABSTRACT

The influence of tower design on damage accumulation in up-wind turbine blades during tower passage is discussed. The fatigue life of a blade is estimated for a tripod tower configuration and a standard mono-tower. The blade stresses are determined from a dynamic mechanical model with a delay effect included in the normal coefficient used to compute the transverse load. Furthermore, the rotational effect of the turbulence spectrum is included in the model. The proposed tripod configuration of the tower limits the damage accumulation in the turbine blades significantly when compared to the fatigue of a blade from a mono-tower wind turbine.

1. INTRODUCTION

1.1 Problem statement

Traditionally, modern wind turbine towers are designed as tubular shell structures as presented in Figure 1 (left). During tower passage of a blade, see Figure 2, the angle of attack α diminishes significantly due to the stagnation of the mean wind U_n in front of the tower. Consequently, the thrust on the blade is reduced and a displacement in opposite direction of the incoming mean wind is observed. This phenomenon (shadow effect) induces a stress reversal, which increases the fatigue damage accumulation in the wind turbine blades. In this paper the impact on damage accumulation is sought reduced with an alternative tripod tower design, see Figure 1

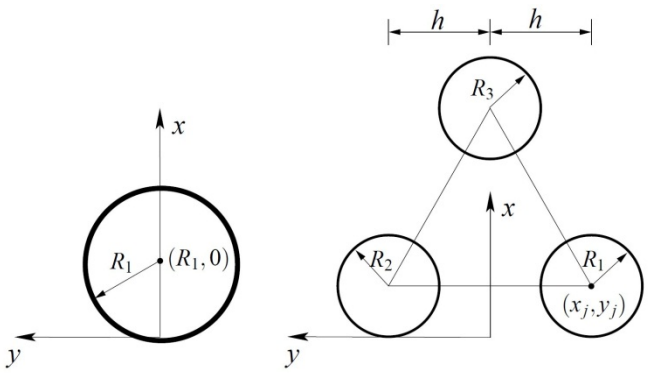

Fig. 1. Two tower configurations, the mono-tower to the left with a larger radius R_1 and $(x_1,y_1)=(R_1,0)$ compared to the tripod legs with radii R_j $(j=1,3)$.

[1] ICOSSAR 09.

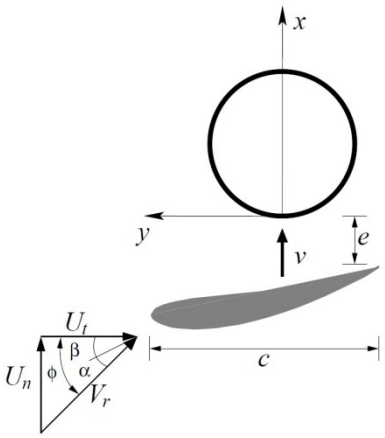

Fig. 2. The tower passage clearance e of the airfoil with the applied wind velocity components.

(right), where the radii $R_1 = R_2 = R_3$ of the individual towers are smaller compared to the standard mono-tower. The stress variation during tower passage depends on the ratio e/R_j, where e is the clearance of the un-deformed blade and R_1 and $R_j (j = 1,3)$ are the radii of the mono-tower and tripod, respectively, see Figure 1. A decreased radius causes a reduced stagnation zone, and therefore the final damage state is expected to be reduced accordingly.

1.2 Shadow effect

The shadow effect has been extensively analyzed in the literature. (Wang & Coton 2001) considered tower shadow for down-wind turbines, where the shadow effect is even more pronounced. (Dolan & Lehn 2006) compared the oscillations of the rotor torque during tower passage and the oscillations due to the mean wind shear using a quasi-static model for the tangential coefficient. They showed that the tower shadow effect contributes more significantly to the oscillations. (Munduate et al. 2004) made wind tunnel experiments with a two-bladed down-wind turbine, and concluded that the delay of non-stationary changes of the angle of attack α has significant impact on the resultant normal coefficient c_n, which effects the transverse load in the x-direction along the blade. This delay effect must be included in the formulation via a memory integral.

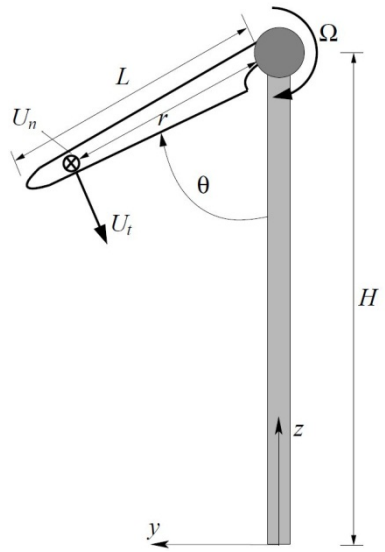

Figure 3. Tower and rotating blade.

2. THE MECHANICAL MODEL

2.1 The wind turbine blade geometry

Figure 3 shows the geometry of a single blade of a horizontal axis up-wind turbine. The height of the tower is H, the length of the blade is L, and the constant speed of the rotor is Ω. The position in the $(y-z)$ rotor plane of a cross section of the blade is defined in polar coordinates (r,θ). The corresponding Cartesian coordinates read:

$$x = -e + v \tag{1}$$

$$y = r\sin(\theta) \tag{2}$$

$$z = H - r\cos(\theta), \tag{3}$$

where θ is the azimuth angle, measured clockwise and zero when the blade is pointing downwards. The displacement of a cross section in the x-direction is denoted $v(r,t)$,

where t is time and r is the radius from the hub. The wind velocity components upstream in the vicinity of the tower(s) are determined from potential flow theory (Milne-Thompson 1996):

$$U_x = U_0 \sum_{j=1}^{n} \left(1 + R_j^2 \frac{(y-y_j)^2 - (x-x_j)^2}{\left((x-x_j)^2 + (y-y_j)^2\right)^2} \right) \tag{4}$$

$$U_y = -2U_0 \sum_{j=1}^{n} \left(R_j^2 \frac{(y-y_j)(x-x_j)}{\left((x-x_j)^2 + (y-y_j)^2\right)^2} \right) \tag{5}$$

where $n=1$ for the mono-tower and $n=2$ for the tripod, respectively, and (x_j, y_j) represents the coordinates of the center of the j th cylinder. The free mean wind speed U_0 at a height z is found from:

$$U_0 = U_{10} k_t \ln \tag{6}$$

where U_{10} is the 5-year return value of the 10-minute mean wind speed at 10m height and the terrain roughness parameters are $z_0 = 0.03$ and $k_t = 0.17$. In this paper the same clearance is used in the blade fatigue analysis for the two towers. In reality the clearance is changed when the nacelle is yawed, and the relative mean wind direction is changed accordingly, which should be included in the analysis as a stochastic variable. The wind velocity components in the tangential and normal directions relative to the moving blade read:

$$U_n = (U_x + u - \dot{v})(1-a) \tag{7}$$

$$U_t = (\Omega r - U_y \cos(\theta))(1-a') \tag{8}$$

where Ω is the rotational velocity of the blade, $\dot{v}$ and u are the velocity of the cross section and the turbulence component in the x-direction, respectively. The induction coefficients a and a' are obtained from the Blade Element Momentum (BEM) theory (Hansen 2001), where the angle of attack $\alpha(r,t)$ is iterated from the the velocity components, induction effects and the pre-twist angle β of the blade at the cross section. In the BEM iteration the instantaneous relative wind speed measured by an observer fixed to the cross section is $V_r = \sqrt{U_n^2 + U_t^2}$ and the angle of attack is obtained from $\alpha = \varphi - \beta - \varphi_p$, where the angle $\phi = \tan^{-1}\left(U_t / U_n\right)$, see Figure 2, and ϕ_p is the pitch angle of the blade, which depends on the wind velocity at hub height (Jonkman et al. 2008).

2.2 Shadow effect

The unsteady effects associated with a tower passage of the blades are important in the estimation of fatigue life. The physical significance behind the phenomena are studied in unsteady aerodynamic experiments (Hand et al. 2001), where data is available as validation to numerical models. During tower passage the mean bending stress is reduced. Due to the aerodynamic damping the stress reversal is relatively small. This means that the shadow effect has minor influence on the extreme load case. The quasi-static normal coefficient $c_n(r,t)$ denotes the normal coefficient, if $\alpha(r,t)$ is constant in time. However, variations $d\alpha$ due to fluctuations of U_n or U_t is only observed in the normal coefficient after a transient period, where the flow conditions re-establish at a new stationary state. The fluctuations of U_n during the tower passage have a resemblance to models for the vertical turbulence on an air-plane wing. Based on these observations (Leishman 2001) considered the time-delay effect on c_n during a tower

passage in a analog model. The present normal coefficient $\bar{c}_n = \bar{c}_n(r,t)$ is obtained from the convolution integral:

$$\bar{c}_n(t) = 2\pi\left(\alpha(0)\psi(t) + \int_0^t \psi(t-\tau)d\alpha(\tau)\right) \tag{9}$$

where $\psi(t)$ is the Küssner function. By means of a rational approximation to this function the solution of the transient normal coefficient may be obtained from (Fung 1993):

$$\bar{c}_n(t) = 2\pi\left(A_1 c_1(t) + A_2 c_2(t)\right) \tag{10}$$

where $A_1 = 0.5$ and $A_2 = 0.5$ are non-dimensional coefficients. The coefficients $c_i\,(i = 1,2)$ are obtained from the 1st order filter equations:

$$\frac{\partial c_i}{\partial t} = \nu_i(\alpha(t) - c_i(t)) \tag{11}$$

where $\nu_i\,(i = 1,2)$ are time scale factors defined as $\nu_1 = 0.26U_t/c$ and $\nu_2 = U_t/c$. The normal load per unit length at the next instant of time is then obtained from:

$$N(r,t+\Delta t) = \frac{1}{2}\rho V_r^2(r,t+\Delta t)\bar{c}_n(r,t+\Delta t)c(r) \tag{12}$$

where Δt is the time step in the numerical integration scheme, ρ is the mass density of air and $c(r)$ is the chord length, see Figure 2.

2.3 Rotational turbulence spectrum

The auto-spectral density of the turbulence component u co-directional to the mean wind velocity U_0 is completely different, when measured in a fixed frame of reference and in a frame of reference fixed to a rotating blade. The one-sided auto-spectral density in a fixed frame has been indicated in Figure 4 with an unbroken line. At large angular frequencies the spectrum approach asymptotically to a linear variation with the slope $5/3$ in a double-logarithmic mapping in agreement with the Kolmogorov equilibrium theory for the inertial subrange. The one-sided auto-spectral density measured in a rotating frame of reference shows marked peaks at the angular frequencies $\omega = \Omega$, $\omega = 2\Omega$ etc. The variance of the spectrum is identical to that of the spectrum in the fixed frame. Hence, the kinetic energy of the turbulence is conceived, but is considerably redistributed in the frequency space. The rotational effect is more pronounced at the tip of the wing and cease at the hub. Since the wind load is concentrated at the outer 1/3 of the blade, this effect is taken into consideration in the model of the blade. The model presented in (Gilling et al. 2009) is here adopted to generate the turbulence wind fields with a turbulence intensity $I_v = 0.16$ in Wind Turbine Class I (IEC 2005). A frozen turbulence box is generated for each mean wind

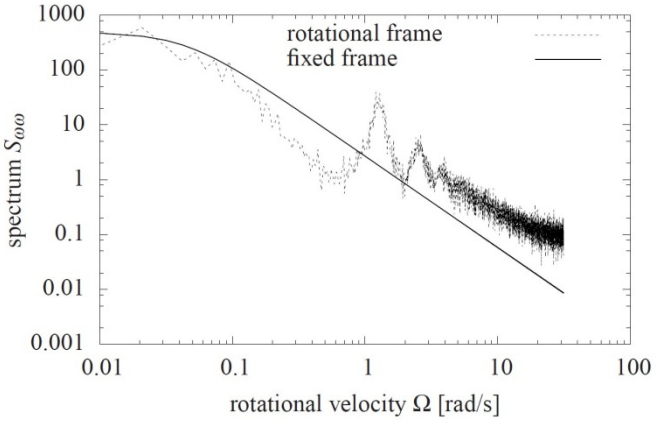

Figure 4. One-sided auto-spectral density of wind turbulence for a fixed and rotating frame of reference.

speed considered in the fatigue analysis, which is converted into the rotor with the mean wind at hub in agreement with Taylor's hypothesis. Next, the turbulence at a given cross section is obtained by interpolation among the grid points of the turbulence box.

2.4 Structural model

The dynamic response of the blade during tower passage is primarily quasi-static and the dynamic effect is confined to the two lowest blade eigen-modes. The dynamic component is relatively small when the boundary layer remain attached, where a substantial aerodynamic damping is present. For this reason only these modes are included in the dynamic analysis. The blade characteristics are taken from a 5MW NREL reference wind turbine (Jonkman et al. 2008), where the blade properties are discretized at 17 points along the blade. The distributions of mass per unit length $\mu(r)$ and the bending stiffness $EI(r)$ are shown in Figure 5 and 6, respectively, and have been used in the modal analysis. The two lowest eigen-modes are shown in Figure 7 and the corresponding eigen-frequencies are listed in Table 1.

Eigen-frequency	ω_1, ω_2	6.32, 30.54	rad/s
Hub height	H	88	m
Mono Tower radius	R_1	3.0	m
Tripod radii ($j = 1,3$)	R_j	1.0	m
Blade length	L	63	m
Hub diameter of blade	D	3.8	m
Clearance	e	4.0	m
Leg distance (tripod)	$2h$	8.0	m
Rotational speed	Ω	1.26	rad/s
Young's modulus	E	$0.05 \cdot 10^{12}$	N/m^2
Bending stiffness	EI	$18114 \cdot 10^6$	Nm^2
Damping ratios	ζ_1, ζ_2	10%,1%	

Table 1. Model characteristics.

The displacement field $v(r,t)$ can be formulated as (Preumont 2002):

$$v(r,t) = \sum \Phi_i(r) q_i(t) + v_{st}(r,t) - \sum \frac{1}{m_i \omega_i^2} \Phi_i(r) F_i(t), \tag{13}$$

in which $v_{st}(r,t)$ is the quasi-static displacement from the load $N(x,t)$, and the last summation withdraws the quasi-static contribution from the two lowest modes. In Equation 13, $\omega_i\,(i = 1,2)$ is the undamped angular flap-wise blade eigen-frequencies, and Φ_i is the related eigen-modes. m_i and $F_i(t)$ denote the modal masses and the modal loads, respectively, and can be computed from:

Figure 5.The mass distribution along the blade.

$$m_i = \int_0^L \mu(x) \Phi_i(x)^2 dx\,. \tag{14}$$

$$F_i(t) = \int_0^L N(x,t) \Phi_i(x) dx\,. \tag{15}$$

The velocity and acceleration at a cross section can be computed from the derivatives of the dynamic part of the response as follows:

$$\dot{v}(r,t) \cong \sum \Phi_i(r) \dot{q}_i(t)$$

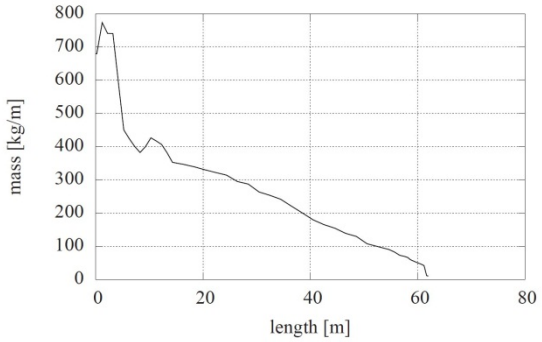

Figure 5. The mass distribution along the blade.

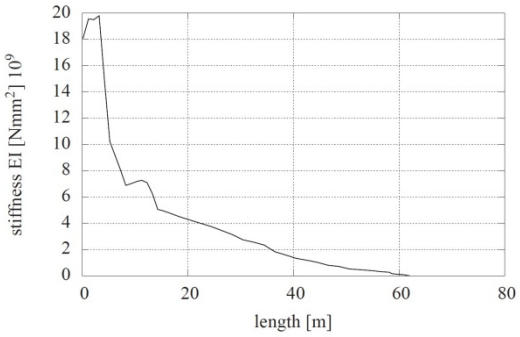

Figure 6. The bending stiffness distribution *EI(r)* along the blade.

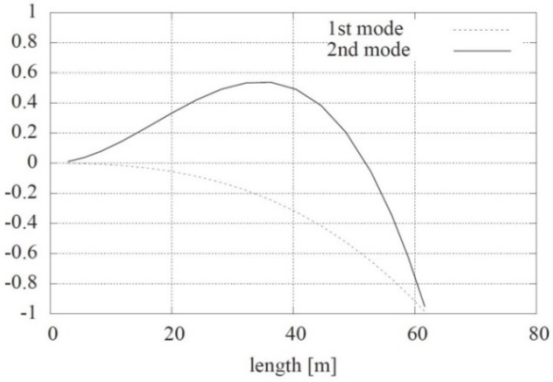

Figure 7. 1st and 2nd blade eigen-modes.

Finally, the modal coordinates for the two modes are given by the differential equation of motion:

$$m_i\left(\ddot{q}_i + 2\zeta_i\omega_i\dot{q}_i + \omega_i^2 q_i\right) = F_i(t)\,. \tag{17}$$

In Equation 17, $\zeta_i\,(i=1,2)$ is the modal damping ratios including both structural and aerodynamic damping. In the analysis aerodynamic damping is only included in the first eigen-mode. The bending moment in the blade at time $(t+\Delta t)$ becomes:

$$M(r,t+\Delta t) = \int_r^L (x-r)N(r,t+\Delta t)dx\,. \tag{18}$$

The corresponding displacement follows from Bernoulli Euler beam theory for a cantilever beam:

1964The quadratures in Equation 19 and 18 have been solved by Simpson integration.

3 ANALYSIS

The expected damage at blade hub is estimated for the mono- and tripod tower, where a lifetime of 20 years is assumed. The blade hub bending moment from Equation 18 is transformed to a normal stress that is used in the fatigue analysis. In the analysis a

range of wind speeds are included with the corresponding probability distribution. Wind speeds at $z = 10\,\text{m}$ included are $U_{10} = [5, 7, .., 19, 21]\,\text{m/s}$. Thus, the turbine runs for all wind speeds at hub height and control systems are not considered. The hub bending moment output from the structural model is shown in Figure 8 for a mean wind $U_{10} = 11\,\text{m/s}$, where only 25 seconds of the time serie is reported.

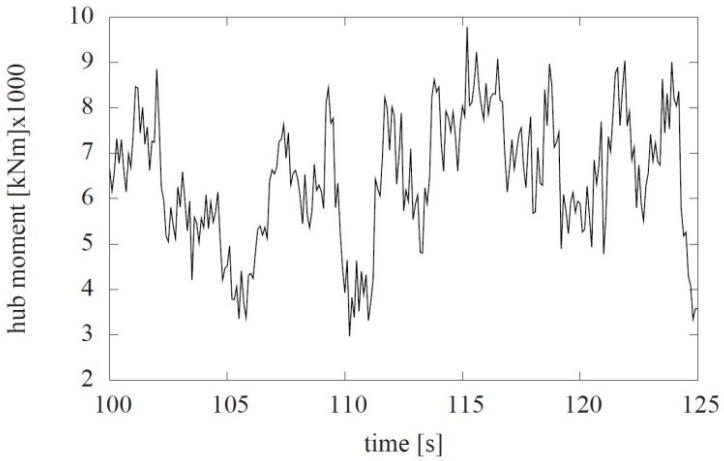

Figure 8. Hub bending moment for a mean wind U_{10}*11m/s.*

3.1 Normal stress at the blade hub

The normal stress at the blade hub for the mono-tower case is presented in Figure 9 for 3 out of the 9 wind speeds considered in the fatigue analysis. The mean wind speed has a significant impact on the mean value and the standard derivation of the stress. Consequently, a wider range of stress amplitudes is experienced at the blade hub, see Figure 12. The corresponding normal stress at the blade hub for the tripod tower configuration is shown in Figure 10. As seen, a lower mean value and standard derivation are obtained compared to the analyses with the mono-tower.

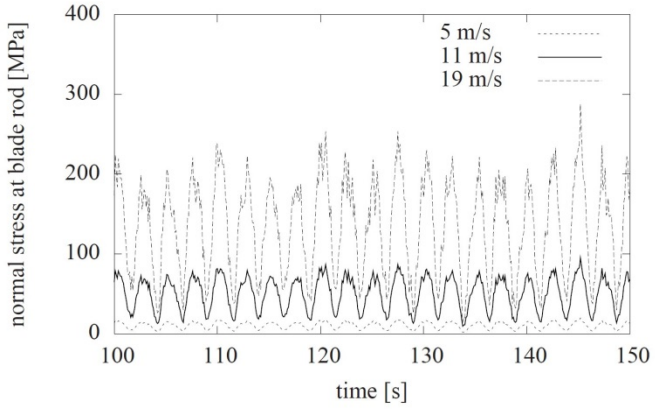

Figure 9. Normal stress at blade hub when a standard mono-tower is used for different wind speeds U_{10}.

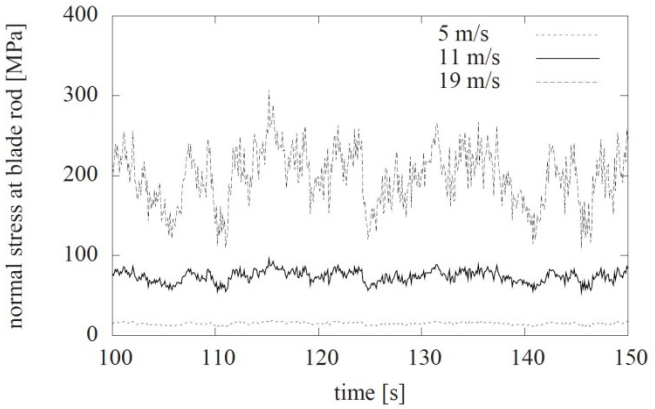

Figure 10. Normal stress at blade hub when the tripod tower system is used for different wind speeds U_{10}.

3.2 Estimation of fatigue life

Fatigue properties of fiberglass composite materials are discussed in (Sutherland & Mandell 2005), where an optimal constant life diagram is proposed. In (Toft & Sørensen 2008) the constant life diagram is further developed, where experimental results from (WMC) is used. The fatigue data used for the fiber material of the blade is taken from (Toft & Sørensen 2008) and reported in constant life diagram in Figure 11. The procedure in the IEC norm (IEC 2005) is followed, where 8 different mean wind speeds are used. The mean damage per unit of time is determined by ergodic sampling over a referential time interval of $T = 600\,\mathrm{s}$.

Figure 12 shows stress cycles and mean stress output from a rain flow counting procedure for a wind speed $U_{10} = 11\,\mathrm{m/s}$. In composite materials not only the stress amplitude but also the mean stress is important for the fatigue life. The stress points are evaluated using the constant life diagram in Figure 11. The R values define the ratio between the maximum and minimum stress in a stress cycle i.e. $R = -1$ means that the maximum tensile stress equals the minimum compressive stress. The expected damage during the lifetime of the wind turbine is computed from:

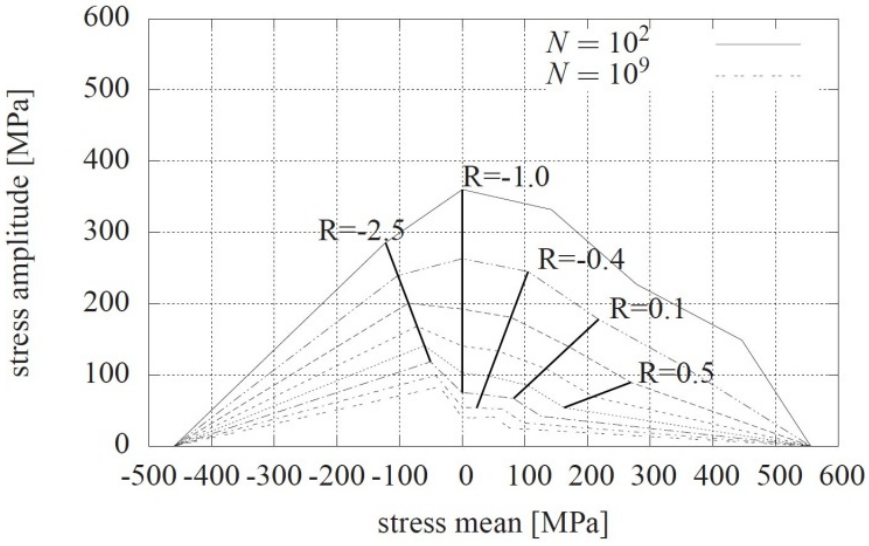

Figure 11. Constant life diagram.

$$E[D] = \frac{\text{Lifetime}}{T}\Bigg(\int_{U_{10}^1}^{U_{10}^2}\int_0^\infty \frac{n_{\text{st}}(\sigma(U_{10},T))}{N} P(U_{10})\, d\sigma dU_{10} \Bigg) \tag{20}$$

where the probability distribution function $P_{U_{10}}$ for the mean wind velocity is given as a Rayleigh distribution (IEC 2005):

$$P_{U_{10}}(u_{10}) = 1 - \exp\left(-\pi \left(\frac{u_{10}}{2V_{\text{avg}}} \right)^2 \right), \tag{21}$$

where $V_{\text{avg}} = 0.2V_{\text{ref}}$ with the reference velocity $V_{\text{ref}} = 50\,\text{m/s}$ for Wind Turbine Class I in (IEC2005). In Equation 20, n_{st} is the number of cycles for the respective wind speeds. The number of cycles are shown in Figure 12. The 9 wind speeds included in the analysis form 8 intervals defining U_{10}^1 and U_{10}^2, which means for $U_{10} = 6\,\text{m/s}$, $U_{10}^1 = 5\,\text{m/s}$ and $U_{10}^2 = 7\,\text{m/s}$. The maximum number of cycles, characteristic for the material exposed to a constant stress range and mean stress, is denoted N in Equation 20, and is determined from the constant life diagram in Figure 11. In Figure 13 the number of cycles for defined stress intervals are presented. For low wind speeds all the cycles are located in the lowest stress interval, whereas in case of a high wind speed different stress amplitudes are experienced. The final expected damage values for the two tower configurations using Equation 20 are shown in Table 2. A lower expected damage is obtained for the tripod system.

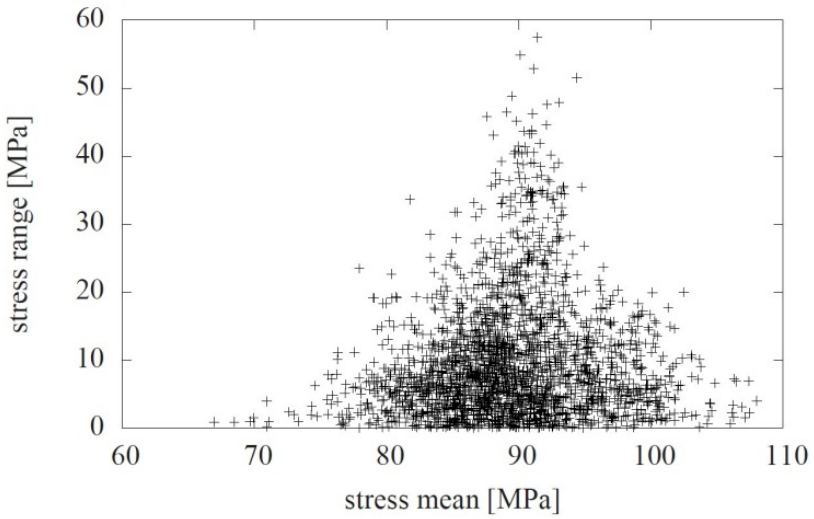

Figure 12. Mean stress and stress range for cycles within a sampling period *T=600s*. Mean wind velocity is U_0*=11m/s*.

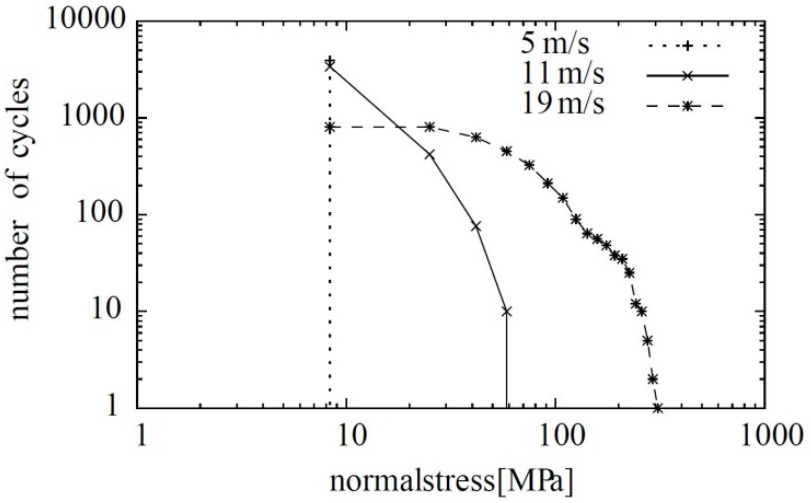

Figure 13. Rain flow counting results showing the number of cycles for different stress intervals in the blade hub using the tripod tower.

Table 2. Expected fatigue life *E(D)* dependent on tower system.

Tower system	$E(D)$
Mono	0.305
Tripod	0.024

4 CONCLUSIONS

Fatigue life of a wind turbine blade is discussed in this paper. A significant contribution to damage accumulation in the blade is caused by the tower passage, due to the stagnation of the wind in front of the tower. Consequently, the thrust on the blade is reduced and a displacement in opposite direction of the incoming mean wind is observed. In this paper, a different tower design is proposed, where this effect is limited. Instead of a mono-tower, a tripod system is used. The expected damage value for the blade is lower compared to the same analysis using a mono-tower. In this analysis, the structural design of the tripod tower (buckling analysis) is not considered and no safety factors are included in the example presented. Furthermore, only one wind direction is included. However, the analysis suggests that the alternative tower design shows promise for improving the fatigue life of the blade.

ACKNOWLEDGEMENTS

S.R.K. Nielsen acknowledge the support of Danish Energy Authority under the grant no. EFPO7-II: "Estimation of Extreme Responses and Failure Probabilities of Wind Turbines under Normal Operations by means of Controlled Monte Carlo Simulations".

REFERENCES

[1] Dolan, D. S. L. & P. W. Lehn (2006). A high resolution tower shadow model for downwind turbines. Journal of Wind Engineering and Industrial Aerodynamics 21, 717–724.

[2] Fung, Y. C. (1993). An Introduction to the Theory of Aeroelasticity. Dover Publications.

[3] Gilling, L., S. R. K. Nielsen & N. N. Sørensen (2009). Generation of synthetic turbulence in arbitrary domains. In M. Dogaki, M. Sakano, and S. Nishimura (Eds.), Proceedings of the 10th International Conference on Structural Safety and Reliability, Kansai University, Japan.

[4] Hand, M., D. Simms, L. Fingersh, D. Jager, J. Cotrell, S. Schreck & S. Larwood (2001). Unsteady aerodynamics experiment phase vi: Wind tunnel test configurations and available data campaigns. Technical Report NREL/TP-500-29955, National Renewable Laboratory.

[5] Hansen, M. O. L. (2001). Aerodynamics of Wind Turbines. James & James.

[6] IEC (2005). Wind turbine -part 1 design requirement. IEC 61400-1:2005(E) 3rd edition.

[7] Jonkman, J., S. Butterfield, W. Musial & G. Scott (2008). Definition of a 5-mw reference wind turbine for offshore system development. NREL/TP500-38060, Golden, CO: National Renewable Energy Laboratory (to be published).

[8] Leishman, J. G. (2001). Challenges in modelling the unsteady aerodynamics of wind turbines. 21st ASME Wind Energy Symposium.

[9] Milne-Thompson, L. M. (1996). Theoretical Aerodynamics. Dover Publications.

[10] Munduate, X., F. N. Coton & R. A. M. Galbraith (2004). An investigation of the aerodynamic response of a wind turbine blade to tower shadow. ASME Journal of Solar Energy Engineering 126, 1034–1040.

[11] Preumont, A. (2002). Vibration Control of Active Structures: An Introduction. Kluwer Academic Publishers.

[12] Sutherland, H. J. & J. F. Mandell (2005). Optimized constant-life diagram for the analysis of fiberglass composites used in wind turbine blades. Journal of Solar Energy Engineering-Transactions of the Asme 127, 563–569.

[13] Toft, H. S. & J. D. Sørensen (2008). Stochastic models for strength of wind turbine blades using tests. In EWEC, Europe's Premier Wind Energy Event, Brussels, Belgium.

[14] Wang, T. & F. N. Coton (2001). A high resolution tower shadow model for downwind turbines. Journal of Wind Engineering and Industrial Aerodynamics 89, 873–892.

[15] WMC. Knowledge centre wmc. http://www.wmc.eu.